

Omni-GAN: On the Secrets of cGANs and Beyond

Peng Zhou¹, Lingxi Xie², Bingbing Ni¹, Qi Tian²

¹Shanghai Jiao Tong University, ²Huawei Inc.

zhoupengcv@sjtu.edu.cn, 198808xc@gmail.com, nibingbing@sjtu.edu.cn,

tian.qil@huawei.com

Abstract

It has been an important problem to design a proper discriminator for conditional generative adversarial networks (cGANs). In this paper, we investigate two popular choices, the projection-based and classification-based discriminators, and reveal that both of them suffer some kind of drawbacks that affect the learning ability of cGANs. Then, we present our solution that trains a powerful discriminator and avoids over-fitting with regularization. In addition, we unify multiple targets (class, domain, reality, etc.) into one loss function to enable a wider range of applications. Our algorithm, named **Omni-GAN**, by proposing a simple modification, improves the projection-based cGAN performance significantly and achieves a new state-of-the-art in generating mid/high-resolution images (a record-breaking IS of 190.9 on ImageNet 128×128). More importantly, we explain experimentally why Omni-GAN is significantly better than the projection-based cGAN, BigGAN, offering new possible directions for optimizing cGANs. Code is available¹.

1. Introduction

Generative Adversarial Networks (GANs) [10] are powerful tools for image generation [1, 15, 24] and domain adaptation [3, 14, 22, 38]. The big family of GANs can be roughly divided into two parts, unconditional GANs [17, 18] and conditional GANs (cGANs) [23, 2], differing from each other in whether the class labels (e.g., face, car, flower, etc.) are used for image generation. It is well acknowledged that cGANs enjoy both higher potentials and higher risks in the training stage. As shown in Fig. 1, BigGAN [2] and Multi-hinge GAN [19], two cGAN variants, achieve higher Inception score (IS) [33] than StyleGAN [18], an unconditional counterpart, but the curves drop dramatically at some point of training (a.k.a. mode collapse). This makes the cGAN training procedure unstable and thus early termina-

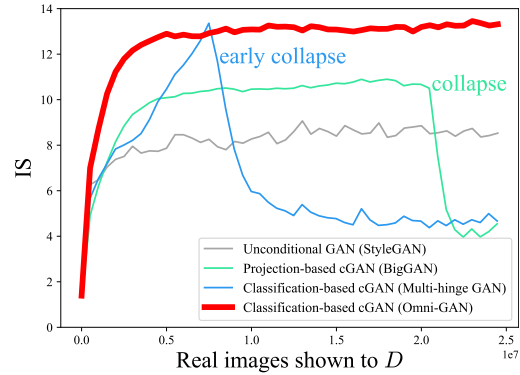


Figure 1: Inception score (IS) of unconditional GANs and conditional GANs on CIFAR100. Omni-GAN enjoys both high generation quality and a low risk of mode collapse.

tion is often required to achieve satisfying performance.

As noticed by the community [16], the instability of the training procedure is highly related to the discriminator, i.e., the module that outputs a probability indicating the reality of the generated image. We further categorize the existing discriminators for cGANs into two types, namely, projection-based [25, 2] and classification-based [27, 19], by whether the discriminator is required to output an explicit class label for each image. We find that, although the former (i.e., projection-based, with a weaker, implicit discriminator) are inferior to the latter in terms of the Inception score, the latter are prone to mode collapse (e.g., in Fig. 1, Multi-hinge GAN achieves a higher Inception score but collapses earlier). This makes us to consider the relationship between the training stability and the strength of the discriminator.

The main discovery of this paper is that classification-based and projection-based discriminator can be unified using a multi-label classification loss [35]. This offers us an opportunity to observe the advantages and disadvantages of both options. As a result, we find that using a strong discriminator (in particular, the classification-based one)

¹<https://github.com/PeterouZh/Omni-GAN-PyTorch>

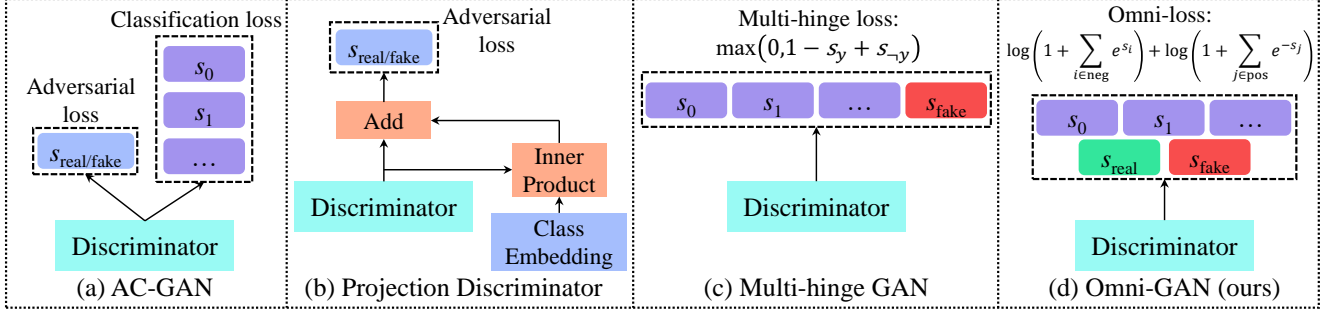


Figure 2: Different discriminator models for cGANs. Omni-loss integrates multiple discrimination tasks (class and reality) into one loss function and thus facilitate both the hyper-parameter tuning and deployment of the algorithm. Please refer to the text (Sec. 2.1 and Sec. 3.1) for more details.

and equipping it with proper regularization (to prevent it from quickly memorizing the training image set) is the best choice, where the GAN model enjoys high quality in image generation yet has a low risk of mode collapse. Based on the strong supervision, regularization is easily added to the classification-based loss function in the form of a weight decay that only requires a few lines of code. We name the proposed algorithm **Omni-GAN**.

Omni-GAN has the ability to integrate multiple discrimination tasks, including object classification, domain classification, and reality judgment (the adversarial term), into one objective, which further simplifies the deployment by getting rid of tuning multiple hyper-parameters. In extensive experiments, we demonstrate the competitive performance of Omni-GAN on (i) CIFAR [20] and ImageNet [7], two standard benchmarks for conditional image generation, (ii) Cityscapes [5], an image-to-image translation task converting a semantic segmentation mask to a photorealistic image, and (iii) the mixed MNIST [21] and SVHN [26] dataset to verify the ability of fitting different domains. Omni-GAN shows a stronger ability in resisting mode collapse, *e.g.*, compared to BigGAN, the safe area (keeping a high Inception score) is augmented by at least two times. These results verify that making full use of supervision can improve the generation quality at the risk of easier mode collapse, yet weight decay, a simple regularization method, is effective to avoid the collapse and thus achieve superior performance.

Our contributions are as follows:

- Our core claim is that the combination of strong supervision and weight decay is the secret of cGANs. Strong supervision is good for fast convergence and high performance but causes cGANs to collapse earlier. Weight decay is effective in avoiding early collapse and thus helps to achieve superior performance.
- We design two types of OmniGANs to show why OmniGAN outperform the projection-based cGANs, *i.e.*,

OmniGAN, which uses a strong classification loss, and **one-sided OmniGAN**, which imitates the way how projection-based cGANs employs class labels (its loss essentially being a weak, implicit classification loss). These two types of OmniGANs enable us to intuitively observe the importance of making full use of class supervision.

- Omni-GAN achieves state-of-the-art results on ImageNet with 128×128 and 256×256 resolution. In particular, using the same network architecture and number of parameters, its IS is almost twice that of BigGAN, namely 190.94 vs. 104.57 on ImageNet 128×128 . Moreover, Omni-GAN only needs one day to reach the IS score of BigGAN which is trained for two weeks using eight v100 GPUs.
- We integrate multiple discrimination tasks into one objective with omni-loss and thus ease both the hyper-parameter tuning and deployment of the algorithm.
- We put forward some new perspectives for improving cGAN training, which may inspire the community to rethink the existing strategies for optimization.

2. Preliminaries

2.1. Conditional GANs

Conditional GAN (cGAN) [23] adds conditional information to the generator and discriminator of GANs. There are some ways to incorporate class information into the generator, such as conditional batch normalization (CBN) [6], conditional instance normalization (CIN) [9, 12], class-modulated convolution (CMConv) [44], *etc.* There are also different ways to add class information to the discriminator. A simple way is to directly concatenate the class information with the input or features from some middle layers [8, 31, 42, 29, 32]. Next, we expound on several slightly complicated methods.

AC-GAN Auxiliary classifier GAN (AC-GAN) [27] uses an auxiliary classifier to enhance the standard GAN model (see Fig. 2a). In particular, the objective function consists of two parts: the GAN loss, \mathcal{L}_{GAN} , and the classification loss, \mathcal{L}_{cls} :

$$\mathcal{L}_{\text{GAN}} = \mathbb{E} [\log P(g = \text{real} | \mathbf{x}_{\text{real}})] + \mathbb{E} [\log P(g = \text{fake} | \mathbf{x}_{\text{fake}})], \quad (1)$$

$$\mathcal{L}_{\text{cls}} = \mathbb{E} [\log P(g = c | \mathbf{x}_{\text{real}})] + \mathbb{E} [\log P(g = c | \mathbf{x}_{\text{fake}})], \quad (2)$$

where g denotes the label of \mathbf{x} . \mathbf{x}_{real} and \mathbf{x}_{fake} represent a real image and a generated image respectively. The discriminator D of AC-GAN is trained to maximize $\mathcal{L}_{\text{GAN}} + \mathcal{L}_{\text{cls}}$, and the generator is trained to maximize $\mathcal{L}_{\text{cls}} - \mathcal{L}_{\text{GAN}}$.

Projection Discriminator Projection discriminator [25] incorporates class information into the discriminator of GANs in a projection-based way (see Fig. 2b). The mathematical form of the projection discriminator is given by

$$D(\mathbf{x}, \mathbf{y}) = \mathbf{y}^T \mathbf{V} f_1(\mathbf{x}; \theta_1) + f_2(f_1(\mathbf{x}; \theta_1); \theta_2), \quad (3)$$

where \mathbf{x} and \mathbf{y} denote the input image and one-hot label vector respectively. \mathbf{V} is a class embedding matrix, $f_1(\cdot; \theta_1)$ is a vector function, and $f_2(\cdot; \theta_2)$ is a scalar function. $\mathbf{V}, \theta_1, \theta_2$ are learned parameters of D . The discriminator D only outputs a scalar for each pair of \mathbf{x} and \mathbf{y} .

Multi-hinge GAN Multi-hinge GAN [19] uses a $C + 1$ dimensional classifier as the discriminator, which is trained by a multi-class hinge loss (see Fig. 2c). Let the classifier be $S : \mathbb{X} \rightarrow \mathbb{R}^{C+1}$, the input image be \mathbf{x} , and the class label be $y \in \{0, 1, \dots, C-1\}$. We use $\mathbf{s} = S(\mathbf{x})$ to denote the score vector of input image \mathbf{x} . The C -th element of \mathbf{s} , $s_C(\cdot)$, indicates the score corresponding to the fake (with indexing starting at 0). The discriminator loss is given by

$$\mathcal{L}_D = \mathbb{E}_{(\mathbf{x}, \mathbf{y}) \sim p_d} [\max(0, 1 - s_y(\mathbf{x}) + s_{-y}(\mathbf{x}))] + \mathbb{E}_{\mathbf{z} \sim p_z, \mathbf{y} \sim p_d} [\max(0, 1 - s_C(G(\mathbf{z}, \mathbf{y})) + s_{-C}(G(\mathbf{z}, \mathbf{y})))] \quad (4)$$

where $s_y(\mathbf{x})$ denotes the element y of vector \mathbf{s} , and $s_{-y}(\mathbf{x}) = \max_{k \neq y} s_k(\mathbf{x})$, $k \in \{0, 1, \dots, C\} \setminus \{y\}$, represents the highest score except $s_y(\mathbf{x})$. The generator loss consists of two parts:

$$\mathcal{L}_G = \lambda \mathcal{L}_{\text{GAN}} + \mathcal{L}_{\text{FM}} \\ = \lambda \mathbb{E}_{\mathbf{z} \sim p_z, \mathbf{y} \sim p_d} [\max(0, 1 - s_y(G(\mathbf{z}, \mathbf{y})) + s_{-y}(G(\mathbf{z}, \mathbf{y})))] + \mathbb{E}_{\mathbf{z} \sim p_z, \mathbf{y} \sim p_d} [S_{\text{feat}}(G(\mathbf{z}, \mathbf{y})) - \mathbb{E}_{\mathbf{x} \sim p_d} [S_{\text{feat}}(\mathbf{x})]]_1, \quad (5)$$

where the former is the multi-hinge adversarial loss, and the latter is a feature matching loss, which is able to alleviate the problem to some extent of training collapse earlier induced by the multi-hinge loss [19]. $S_{\text{feat}}(\cdot)$ denotes extracting features by the classifier S .

2.2. Unified Loss for Feature Learning

In fact, there is a unified perspective for classification tasks. We denote the positive scores as $\{s_1^{(p)}, s_2^{(p)}, \dots, s_K^{(p)}\}$, and negative scores as $\{s_1^{(n)}, s_2^{(n)}, \dots, s_L^{(n)}\}$, respectively. Sun *et al.* [36] proposed a unified loss to maximize $s^{(p)}$ as well as to minimize $s^{(n)}$. The loss is defined as

$$\mathcal{L}_{\text{uni}} = \log \left[1 + \sum_{i=1}^K \sum_{j=1}^L \exp \left(\gamma (s_j^{(n)} - s_i^{(p)} + m) \right) \right] \\ = \log \left[1 + \sum_{j=1}^L \exp \left(\gamma (s_j^{(n)} + m) \right) \sum_{i=1}^K \exp \left(\gamma (-s_i^{(p)}) \right) \right], \quad (6)$$

where γ stands for a scale factor, and m for a margin between positive and negative scores. Eq. (6) can be converted into triplet loss [34] or softmax with the cross-entropy loss (please refer to [36]).

3. Omni-GAN

In this section, we expound on Omni-GAN. Firstly, we define the omni-loss and show its ability to unify classification-based and projection-based cGANs (Sec. 3.1). Secondly, we show that the classification-based cGAN, Omni-GAN, suffers from early collapse problem existing in other classification-based cGANs such as Multi-hinge GAN. We propose a simple yet effective regularization to overcome this problem (Sec. 3.2). Subsequently, in Sec. 3.3, we evaluate a projection-based variant, one-sided Omni-GAN, substantiating that the superiority of Omni-GAN comes from fully utilizing class supervision. Finally, we show how to apply omni-loss to a fully convolutional discriminator (Sec. 3.4).

3.1. Unifying Classification-based and Projection-based cGANs

We commence from defining the omni-loss. Let \mathbf{x} and \mathbf{y} denote an image and its multi-label vector respectively. S is a classifier. Suppose that there are K positive labels and L negative labels. Then $\mathbf{s} = S(\mathbf{x})$ is a $K + L$ dimensional score vector. The omni-loss is defined as

$$\mathcal{L}_{\text{omni}}(\mathbf{x}, \mathbf{y}) = \log \left(1 + \sum_{i \in \mathbb{I}_{\text{neg}}} e^{s_i(\mathbf{x})} \right) + \log \left(1 + \sum_{j \in \mathbb{I}_{\text{pos}}} e^{-s_j(\mathbf{x})} \right), \quad (7)$$

where \mathbb{I}_{neg} is a set consisting of indexes of negative scores (i.e., $|\mathbb{I}_{\text{neg}}| = L$), and \mathbb{I}_{pos} consists of indexes of positive scores (i.e., $|\mathbb{I}_{\text{pos}}| = K$). $s_k(\mathbf{x})$ represents the element k of vector \mathbf{s} . Next, we introduce two cases of combining omni-loss with cGANs.

The classification-based case. Combining omni-loss with the discriminator of cGANs derives a classification-based cGAN, **Omni-GAN**. We first elucidate the loss of the discriminator. The discriminator loss consists of two parts, one for \mathbf{x}_{real} (drawn from the training data), and the other for \mathbf{x}_{fake} (drawn from the generator). For \mathbf{x}_{real} , its multi-label vector is given by

$$\mathbf{y}_{\text{real}} = [\underbrace{0, \dots, 1_{\text{gt}}, \dots, 0}_C, \underbrace{1_{\text{real}}, 0}_2], \quad (8)$$

whose dimension is $C + 2$, with C being the number of classes of the training dataset. 1_{gt} is 1 if its index in the vector is equal to the ground truth label of \mathbf{x}_{real} , otherwise 0. We use 1 to denote the corresponding score belongs to the positive set, and 0 to the negative set. The multi-label vector of \mathbf{x}_{fake} is also a $C + 2$ dimensional vector:

$$\mathbf{y}_{\text{fake}} = [\underbrace{0, \dots, 0, \dots, 0}_C, \underbrace{0, 1_{\text{fake}}}_2], \quad (9)$$

where in this case it is a one-hot vector with only the last element being 1.

According to Eq. (7), (8), and (9), we define the discriminator loss as

$$\mathcal{L}_D = \mathbb{E}_{\mathbf{x}_{\text{real}} \sim p_d} [\mathcal{L}_{\text{omni}}(\mathbf{x}_{\text{real}}, \mathbf{y}_{\text{real}})] + \mathbb{E}_{\mathbf{x}_{\text{fake}} \sim p_g} [\mathcal{L}_{\text{omni}}(\mathbf{x}_{\text{fake}}, \mathbf{y}_{\text{fake}})], \quad (10)$$

where p_d is the training data distribution, and p_g is the generated data distribution. In this setting, the discriminator D actually acts as a multi-label classifier, which takes as input \mathbf{x} , and outputs a score vector $\mathbf{s} = D(\mathbf{x})$.

The generator attempts to fool the discriminator into believing its samples are real. To this end, its multi-label is set to

$$\mathbf{y}_{\text{fake}}^{(G)} = [\underbrace{0, \dots, 1_G, \dots, 0}_C, \underbrace{1_{\text{real}}, 0}_2], \quad (11)$$

which is the same as \mathbf{y}_{real} defined in Eq. (8). 1_G is 1 if its index in the vector is equal to the label adopted by the generator to generate \mathbf{x}_{fake} , otherwise 0. The generator loss is then given by

$$\mathcal{L}_G = \mathbb{E}_{\mathbf{x}_{\text{fake}} \sim p_g} [\mathcal{L}_{\text{omni}}(\mathbf{x}_{\text{fake}}, \mathbf{y}_{\text{fake}}^{(G)})]. \quad (12)$$

The projection-based case. We imitate the way how the projection-based discriminator [25] utilizes class labels (see Eq. (3)), and design a projection-based variant of Omni-GAN, named **one-sided Omni-GAN**, which does not fully utilize the class supervision.

It is easy to implement one-sided Omni-GAN: only slightly modify the multi-label vector, \mathbf{y} . Following the setting above, the multi-label vector for \mathbf{x}_{real} is set to

$$\mathbf{y}_{\text{real}} = [\underbrace{-1, \dots, 1_{\text{gt}}, \dots, -1}_C, \underbrace{1, -1}_2], \quad (13)$$

where 1_{gt} is 1 if its index in the vector is equal to the ground truth label of \mathbf{x}_{real} , otherwise -1 . And -1 means that the corresponding score will be ignored when calculating the omni-loss. The multi-label vector for \mathbf{x}_{fake} is given by

$$\mathbf{y}_{\text{fake}} = [\underbrace{-1, \dots, 0_G, \dots, -1}_C, \underbrace{0, -1}_2], \quad (14)$$

where 0_G is 0 if its index in the vector is equal to the label adopted by the generator to generate \mathbf{x}_{fake} , otherwise -1 . The discriminator loss is the same as that defined in Eq. (10).

For generator, its multi-label vector for \mathbf{x}_{fake} is

$$\mathbf{y}_{\text{fake}}^{(G)} = [\underbrace{-1, \dots, 1_G, \dots, -1}_C, \underbrace{1, -1}_2], \quad (15)$$

where 1_G is 1 if its index in the vector is equal to the label adopted by the generator to generate \mathbf{x}_{fake} , otherwise -1 . The generator loss is the same as that defined in Eq. (12).

In summary, we introduce two types of omni-GAN, which are derived by modifying the multi-label vector of the omni-loss (defined in Eq. (7)). It is easy to implement the omni-GAN in practice: as shown in Fig. 2d, first, let the discriminator output a vector instead of a scalar; second, apply the omni-loss to the output vector.

3.2. Avoiding Early Collapse

Like other classification-based cGANs, the Omni-GAN also suffers from early collapse during training. We conducted control experiments on CIFAR100 [20], and compared Omni-GAN with a projection-based cGAN, namely BigGAN [2]. As shown in Fig. 3a, the IS of the Omni-GAN shows a very exciting upward trend compared to the projection-based cGAN. However, unfortunately, the IS drops dramatically when about $1M$ real images (20 epoch) are shown to the discriminator, indicating that the training collapses earlier. The projection-based cGAN, BigGAN, also collapses when about $20M$ real images are shown to the discriminator (around 400th epoch).

What causes the collapse? Karras *et al.* [16] found that the discriminator overfits the training dataset, which will lead to incorrect gradients provided to the generator, so that the training diverges. To verify that the collapse of the above projection-based cGAN is due to the over-fitting of the discriminator, we plotted the scalar output of the discriminator, $D(\mathbf{x})$, over the course of training. We utilized the test set of CIFAR100 containing 10,000 images as the verification set, which was not used in the training.

As shown in Fig. 3b, obviously, as training progresses, the $D(\mathbf{x})$ of the validation set tends to that of the generated images, substantiating that the discriminator overfits the training data. We also plotted the FID curve in the same

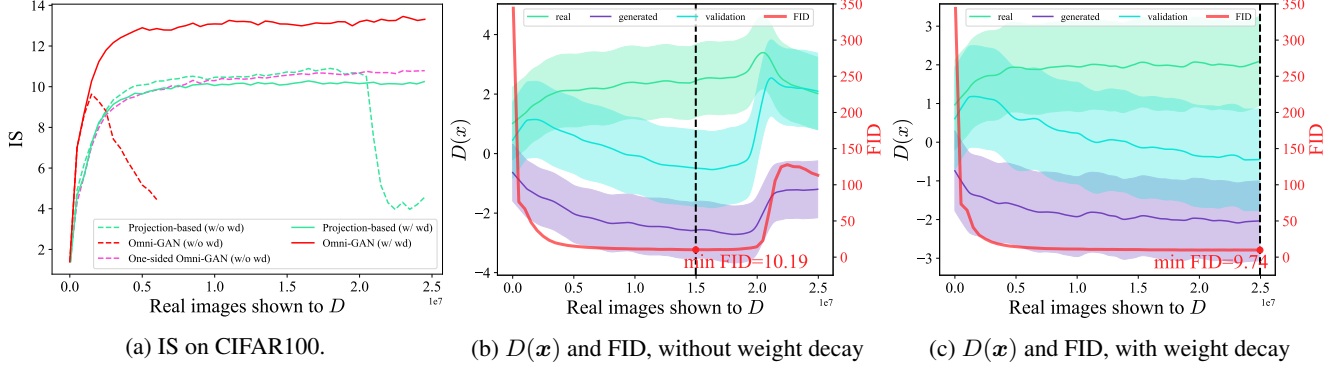


Figure 3: (a) Weight decay can protect Omni-GAN from early collapse while maintaining high performance. (b, c) The raw logits of $D(x)$ and the corresponding FID score of a projection-based cGAN are plotted in the same figure. The black dashed line indicates where the minimum FID is reached. The figures of $D(x)$ are inspired by [16].

figure. It can be seen that when show about $20M$ real images (*i.e.*, around 400 epoch) to the discriminator, the training commences diverging. The best FID is obtained when approximately $15M$ real images are shown to the discriminator.

How to avoid the collapse? To overcome the over-fitting of the discriminator, Karras *et al.* [16] proposed to use data augmentation, a standard solution against over-fitting. In this paper, we propose to apply weight decay to the discriminator to alleviate the over-fitting of the discriminator. In Fig. 3c, we show the $D(x)$ and FID after applying weight decay to the projection-based discriminator. We can find that although the discriminator still overfits the training data, the training dose not collapse during the whole training process (the minimum FID, 9.74, is not reached until the end of the training).

Since weight decay can stabilize the training of the projection-based cGAN, can it stabilize the training of the Omni-GAN? We then applied weight decay to the discriminator of Omni-GAN, and plotted the IS curve in Fig. 3a. Excitingly, the early collapse disappears immediately, and the training process becomes very stable. Moreover, the IS is significantly better than the baseline methods (projection-based cGAN, BigGAN, with or without weight decay).

3.3. The Devil Lies in Supervision

Although the IS of Omni-GAN is much higher than that of the projection-based cGAN (BigGAN), the key factor driving this improvement is still unknown. We proceed to evaluate the one-sided Omni-GAN. One-sided Omni-GAN belongs to projection-based cGANs in that it does not fully utilize the class supervision. To compare fairly with the BigGAN, one-sided Omni-GAN did not use weight decay.

Fig. 3a shows the IS curve of one-sided Omni-GAN. We deliver two messages: one-sided Omni-GAN does not suffer from early collapse even if weight decay is not adopted; the IS of one-sided Omni-GAN is comparable to that of the

projection-based cGAN (BigGAN), but it is worse than that of Omni-GAN. These phenomena substantiate that the notable performance of Omni-GAN comes from making full use of class supervision.

To sum up, our results reveals that fully utilizing the supervision can improve performance of cGANs, but at the risk of early collapse. This work offers a practical way (adding regularization) to overcome the collapse issue (there may exist other ways to achieve the same goal), so that the trained model enjoys both superior performance and safe optimization.

3.4. Generalization to Image-to-Image Translation

Omni-loss can be applied to a fully convolutional discriminator, which is widely adopted by image-to-image translation tasks [28, 13, 40]. As shown in Fig. 4, the discriminator is a fully convolutional network, which takes as input images and outputs feature maps with the number of channels being $C + 2$. C represents the number of classes which is analogous to that of the semantic segmentation task. 2 indicates there are two extra feature maps representing to what extent the input image is real or fake.

We adopt nearest neighbor downsampling to downsample the label map to the same resolution as the output feature maps of the discriminator. Then we use the downsampled label map as ground truth label, and apply a per-pixel omni-loss to the output feature maps of the discriminator. In Sec. 4.3, we will show that the per-pixel omni-loss can improve the performance of semantic image generation [39, 30].

4. Experiments

4.1. Evaluation and Implementation Details

Evaluation. We use Inception Score (IS) [33] and Fréchet Inception Distance (FID) [11] to measure the performance of GANs. In particular, we randomly generate $50K$ images

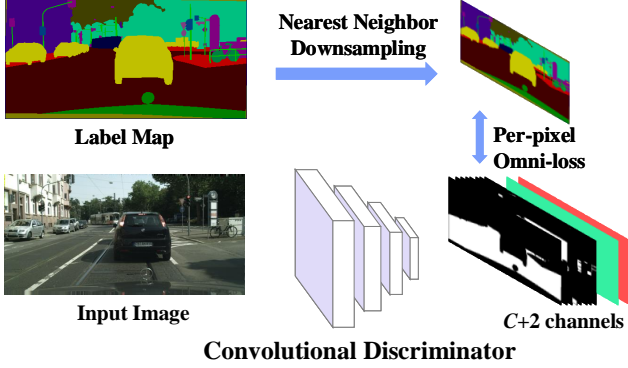


Figure 4: Combine omni-loss with a fully convolutional discriminator whose outputs are feature maps. In the figure, the green and red feature maps represent scores that the input images are real and fake, respectively. Omni-loss is applied to the output feature maps pixel-by-pixel.

and use the official TF inception v3 model [37] to calculate the metrics. The FID statistic files are pre-calculated using all training images. For semantic image synthesis, we follow the evaluation protocol adopted by previous works [4, 40, 28]. Specifically, we use a pre-trained semantic segmentation model to predict the semantic map of the synthesized images, and then use the mean Intersection-over-Union (mIoU) to measure the segmentation performance. The mIoU is used as the performance metric of the synthesized images.

Implementation Details. For cGAN model, we use BigGAN² as our baseline which employs a projection-based discriminator by default. We replace the unofficial evaluation code (*i.e.*, using the PyTorch inception network to calculate IS and FID) with the official evaluation code (using the TF model) to monitor the training process. However, for ImageNet, we directly use the unofficial evaluation code for reasons of efficiency. For semantic image synthesis, we use SPADE³ as our baseline. Hyperparameters are consistent with those of baselines.

4.2. Class-Conditional Image Generation

We first verify the effectiveness of Omni-GAN on the task of class-conditional image generation.

CIFAR10 and CIFAR100. We re-implemented SN-GAN, BigGAN, Multi-hinge GAN, FQ-GAN, and used the official evaluation code to monitor the training process. As shown in Table 1, Omni-GAN achieves both superior FID and IS at the same time on CIFAR10 and CIFAR100. However, there exists a trade-off between FID and IS for other methods. For example, although the classification-based cGAN, Multi-hinge GAN, achieves prominent IS on CI-

Method	CIFAR10		CIFAR100	
	FID ↓	IS ↑	FID ↓	IS ↑
SN-GAN [24]	15.73	8.19	18.87	8.19
AC-GAN [27]	19.70 [†]	8.22 [†]	25.40 [†]	8.80 [†]
<i>cproj</i> [25]	17.50 [†]	8.62 [†]	23.20 [†]	9.04 [†]
BigGAN [2]	7.05	9.14	10.18	10.89
Multi-hinge [19]	6.22	9.55	14.62	13.35
FQ-GAN [43]	6.16	9.16	8.23	10.62
ADA [16]	2.67[†]	10.06[†]	-	-
Omni-GAN (one-sided)	6.98	9.07	8.28	10.99
Omni-GAN	5.52	9.63	8.14	13.51

Table 1: FID and IS on CIFAR10 and CIFAR100. Note that ADA used a larger network than ours (512 vs. 256, feature maps for all layers). [†] indicates quoted from the paper.

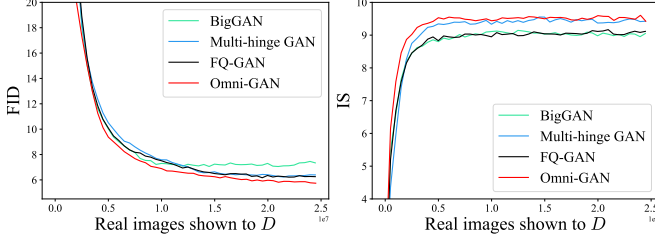
FAR10 and CIFAR100, it gets an inferior FID of 14.62 on CIFAR100. On the other hand, FQ-GAN, which employs a projection discriminator, achieves prominent FID scores, but its IS are ordinary on both CIFAR10 and CIFAR100. Another interesting point is that the performance of one-sided Omni-GAN is worse than that of Omni-GAN, but on par with that of BigGAN. This shows that the excellent performance of Omni-GAN comes from the full use of class supervision. We will comprehensively compare Omni-GAN with BigGAN and Multi-hinge GAN in the discussion (refer to Sec. 5.2, 5.3).

In Table 1, the ADA [16] has more parameters and has been trained for a longer time than Omni-GAN. Besides, it employs data augmentation during the training process. We have tried to combine omni-loss with ADA, but failed. ADA uses the network architecture of StyleGAN2 [18], which employs equalized learning rate technology [15] (explicitly scales the weights at runtime) during the training process. We found that this technique conflicts with weight decay, which is the key to Omni-GAN to avoid early collapse. Combining strong classification loss, such as omni-loss, with StyleGAN while avoiding early collapse still needs further exploration.

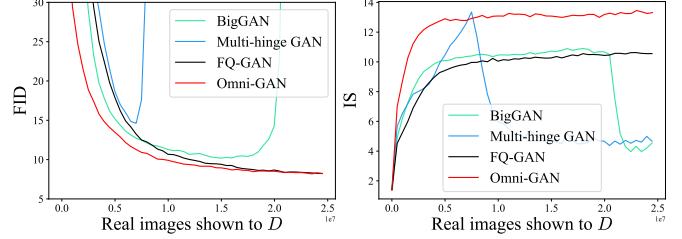
Fig. 5 shows the curves of evaluation scores over the course of training. Obviously, Multi-hinge GAN suffers early collapse on CIFAR100, but not on CIFAR10. We think the reason may be that CIFAR100 has fewer images per class than CIFAR10 (*i.e.*, 500 vs. 5000), in which case the discriminator is more likely to overfit the training data. We will discuss using weight decay to solve this early collapse problem of Multi-hinge GAN in Sec. 5.3. Fig. 5 also shows that Omni-GAN has achieved stable and superior performance on FID and IS at the same time. Considering its simplicity (just changing the loss function of the discriminator), we think Omni-GAN has a potential to be applied in other fields (*e.g.*, super-resolution, image-to-image translation).

²<https://github.com/ajbrock/BigGAN-PyTorch>

³<https://github.com/NVlabs/SPADE>



(a) FID and IS on CIFAR10



(b) FID and IS on CIFAR100

Figure 5: Omni-GAN achieves superior FID and IS at the same time. FQ-GAN looks good in terms of FID but with ordinary IS. Multi-hinge GAN is not stable and crashes on CIFAR100.

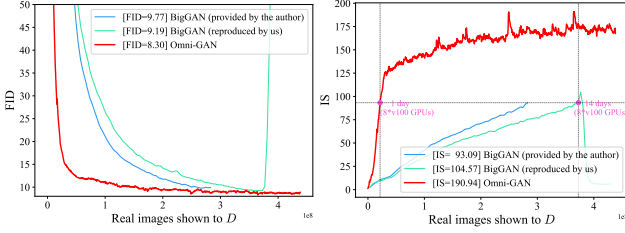


Figure 6: FID and IS on ImageNet 128×128 . Omni-GAN converges faster than the projection-based cGAN, BigGAN. In particular, Omni-GAN only took one day to reach the IS of BigGAN trained for 14 days. Omni-GAN consistently outperforms BigGAN in terms of FID and IS. Its IS is almost twice that of BigGAN, namely 190.94 vs. 104.57, and its FID is also better than BigGAN, namely 8.30 vs. 9.19.

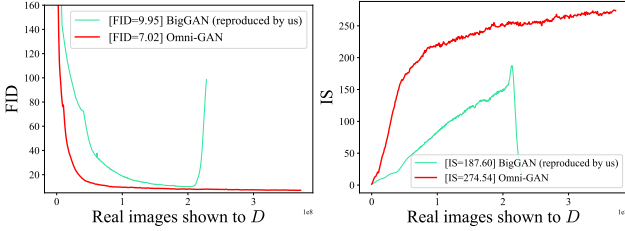


Figure 7: FID and IS on ImageNet 256×256 . Omni-GAN converges faster than BigGAN and shows an astonishing IS compared to the projection-based cGAN, BigGAN.

ImageNet. ImageNet [7] is a large dataset with 1000 number of classes and approximate $1.2M$ training data.

We first reproduced BigGAN on ImageNet with 128×128 resolution and trained it for 335 epochs using eight v100 GPUs, which took 17 days plus 21 hours. As shown in Fig. 6, BigGAN began to collapse at the 294th epoch. Then we train Omni-GAN using the same network architecture as BigGAN. To see if Omni-GAN will collapse like BigGAN, we trained it for more epochs (up to 350 epochs, taking 24 days plus 16 hours). We did not observe mode collapse for Omni-GAN. Omni-GAN shows significant advantages over BigGAN, both in terms of convergence speed and final performance. For example, as shown in Fig. 6, Omni-GAN

Method	ImageNet 128×128		ImageNet 256×256	
	FID ↓	IS ↑	FID ↓	IS ↑
BigGAN [†] [2]	9.77	93.09	-	-
BigGAN [*]	9.19	104.57	9.95	187.60
Omni-GAN	8.30	190.94	7.02	274.54

Table 2: FID and IS on ImageNet dataset. Omni-GAN achieves consistent improvements in terms of FID and IS. It is worth noting that Omni-GAN almost doubles the IS of BigGAN on ImageNet 128×128 experiments, namely from 104.57 to 190.94. Omni-GAN uses the same generator and discriminator (with minor modification for the output layer for the omni-loss) as BigGAN. Therefore, the performance gain does not come from the network architecture or capacity, but from the training strategy that combines strong classification loss (*i.e.*, omni-loss, for excellent performance) and weight decay (to avoid early collapse). [†] indicates the model is provided by the author. ^{*} indicates our reproduced BigGAN using the author’s code.

only took one day to reach the IS of BigGAN trained for 14 days on ImageNet 128×128 . Its IS is almost twice that of BigGAN, namely 190.94 vs. 104.57.

Fig. 7 shows the results of ImageNet 256×256 experiments, which require much longer training time. For example, it took about thirty days to train the BigGAN using eight v100 GPUs, and then the BigGAN began to collapse. Omni-GAN enjoys faster convergence and superior performance than BigGAN in terms of both IS and FID. To see if Omni-GAN will collapse, we trained Omni-GAN for more epochs and no mode collapse is observed.

Table 2 shows the results on ImageNet dataset. Omni-GAN is consistently better than the projection-based cGAN, BigGAN. Notably, Omni-GAN almost doubles the IS of BigGAN on ImageNet 128×128 experiments, namely from 104.57 to 190.94. Considering the huge performance improvement and fast convergence speed of Omni-GAN, we think it is time for the community to use classification-based cGAN, *e.g.*, Omni-GAN, to replace the widely used projection-based cGAN.

SPADE [28]	<i>road</i>	<i>sidewalk</i>	<i>building</i>	<i>wall</i>	<i>fence</i>	<i>pole</i>	<i>traffic light</i>	<i>traffic sign</i>	<i>vegetation</i>	<i>terrain</i>
	97.44	79.89	87.86	50.57	47.21	35.90	38.97	44.67	88.15	66.14
	<i>sky</i>	<i>person</i>	<i>rider</i>	<i>car</i>	<i>truck</i>	<i>bus</i>	<i>train</i>	<i>motorcycle</i>	<i>bicycle</i>	mIoU
	91.61	62.27	38.67	88.68	64.96	70.17	41.42	28.58	58.86	62.21
+ Omni-GAN	<i>road</i>	<i>sidewalk</i>	<i>building</i>	<i>wall</i>	<i>fence</i>	<i>pole</i>	<i>traffic light</i>	<i>traffic sign</i>	<i>vegetation</i>	<i>terrain</i>
	97.57	81.62	88.58	53.39	50.47	35.88	41.08	46.75	89.31	67.00
	<i>sky</i>	<i>person</i>	<i>rider</i>	<i>car</i>	<i>truck</i>	<i>bus</i>	<i>train</i>	<i>motorcycle</i>	<i>bicycle</i>	mIoU
	92.14	63.97	41.99	89.91	71.06	74.21	56.16	33.99	61.23	65.07

Table 3: Semantic image synthesis using SPADE. Replacing the GAN used by SPADE with Omni-GAN can improve the quality of synthesized images.

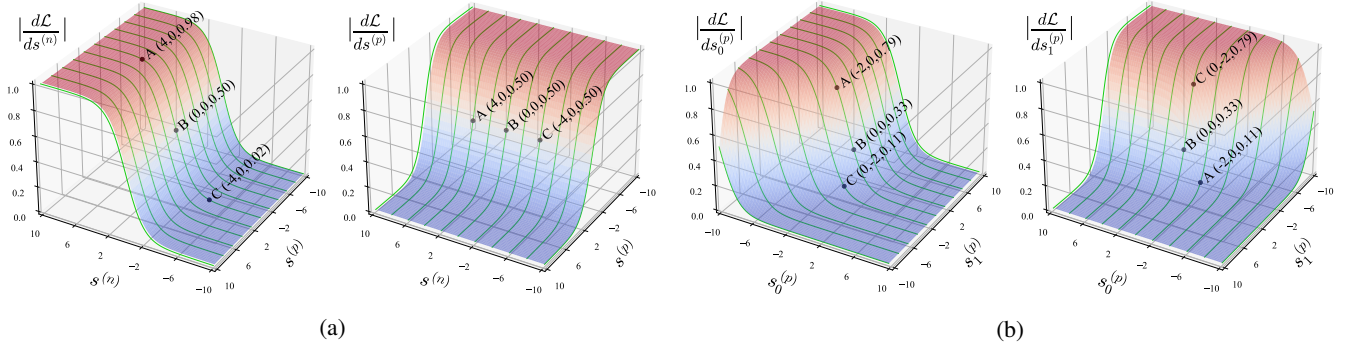


Figure 8: Gradients of the omni-loss. (a) Gradients w.r.t. $s^{(n)}$ and $s^{(p)}$ are independent. (b) Gradients w.r.t. $s_k^{(p)}$, $\{k = 0, 1, \dots\}$, are automatically balanced. Please see the text in Sec. 5.1 for details. This figure is inspired by [36].

4.3. Semantic Image Synthesis

Omni-loss can be easily extended to a fully convolutional discriminator. We show its effectiveness on semantic image synthesis which is an image-to-image task. We use Cityscapes dataset [5] as a testbed, and train models on the training set with size of 2,975. The images is resized to 256×512 . We use SPADE [28] method as our baseline and replace its loss of the discriminator with omni-loss to derive our method. Models are evaluated by the mIoU of the generated images on the test set with 500 images. We use a pre-trained DRN-D-105 [41] as the segmentation model for the sake of evaluation. As shown in Table 3, Omni-GAN improves the mIoU score of SPADE from 62.21 to 65.07, substantiating that the synthesized images possess more semantic information. We believe that the improvement comes from the improved ability of the discriminator in distinguishing different classes, so that the generator receives better guidance and thus produces images with richer semantic information.

4.4. Cross-domain Generation

Omni-loss is essentially a multi-label classification loss [35] and naturally supports classification with multiple positive labels. We have verified the setting with two positive labels above (classification and reality). To further verify the ability of omni-loss to multi-label classification, we constructed a mixed dataset containing images of digits

from two distinct domains, namely MNIST [21] of handwritten digits and SVHN [26] of house numbers in Google Street View images. In this setting, the discriminator needs to predict three attributes, class (recognizing digits), domain, and reality. Due to the limited space, please refer to Appendix B for more experimental details.

5. Discussion

5.1. Gradient Analysis

The gradients of omni-loss have two properties: on one hand, the gradients w.r.t. $s^{(n)}$ and $s^{(p)}$ are independent; on the other hand, the gradients w.r.t. $s_k^{(p)}$ (or $s_k^{(n)}$), $\{k = 0, 1, \dots\}$, are automatically balanced. To illustrate these properties, we visualize the gradients of omni-loss. Fig. 8a shows a case that only contains one $s^{(n)}$ and one $s^{(p)}$. A, B, and C have the same $s^{(p)}$, which is 0, but different $s^{(n)}$ (i.e., 4, 0, -4, respectively). As a result, the gradients w.r.t. $s^{(p)}$ at these three points are the same (i.e., 0.5). Nevertheless, the gradients w.r.t. $s^{(n)}$ at these three points are different. For example, the gradient w.r.t. $s^{(n)}$ at A is largest (equal to 0.98). The reason for this is that the objective of omni-loss is to minimize $s^{(n)}$. Thus the larger the $s^{(n)}$, the larger the gradient w.r.t. $s^{(n)}$.

In Fig. 8b, we show the ability of omni-loss to automatically balance gradients. We consider a case with only two positive labels, namely $s_0^{(p)}$ and $s_1^{(p)}$. Note that this case

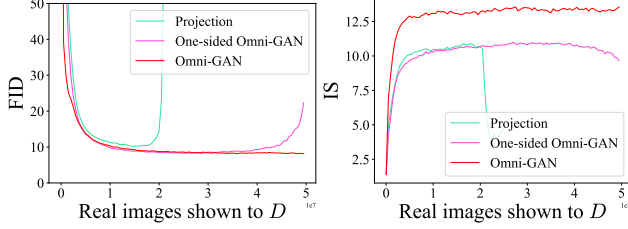


Figure 9: Double the training time to observe when one-sided Omni-GAN crashes on CIFAR100.

is the same as that of one-sided Omni-GAN. We can observe that for A , its $s_0^{(p)}$ is smaller than $s_1^{(p)}$ (i.e., -2 vs. 0). As a result, the gradients w.r.t. $s_0^{(p)}$ is larger than that w.r.t. $s_1^{(p)}$ (i.e., 0.79 vs. 0.11), meaning that the omni-loss try to increase $s_0^{(p)}$ with higher superiority. A similar analysis applies to C as well. For B , since $s_0^{(p)}$ and $s_1^{(p)}$ are equal, the gradients of them are also equal (0.33).

5.2. Comparison with Projection-based GAN

We have shown in Sec. 3.1 that Omni-GAN can be degraded into one-sided Omni-GAN. In this section, we compare one-sided Omni-GAN and projection-based GAN (in particular, BigGAN) on CIFAR100. As shown in Fig. 9, obviously, the IS of one-sided Omni-GAN is worse than that of Omni-GAN, but is comparable with that of projection-based GAN. The reason is that Omni-GAN makes full use of class supervision. However, both one-sided Omni-GAN and the projection-based GAN work in a weaker supervision manner. The same phenomenon still exists on CIFAR10 (refer to Appendix C).

Another interesting phenomenon is that one-sided Omni-GAN collapsed later than the projection-based GAN. In the experiments, we doubled the training time to observe when one-sided Omni-GAN collapses. Fig. 9 shows that one-sided Omni-GAN commences collapsing at a time when about 40M real images is shown to the discriminator, the number which is twice than that of projection-based GAN (about 20M). Note that we did not impose any regularization (e.g., weight decay) on the one-sided Omni-GAN. We think this can be attributed to the characteristic omni-loss owns of balancing gradients automatically (discussed in Sec. 5.1).

5.3. Comparison with Multi-hinge GAN

Multi-hinge GAN belongs to classification-based cGANs, and also suffers from the early collapse issue. In this section, we study whether weight decay is still an effective regularization for Multi-hinge GAN. As shown in Fig. 10, weight decay can indeed make Multi-hinge GAN avoid early collapse. However, the IS of Multi-hinge GAN combined with weight decay is worse than that of

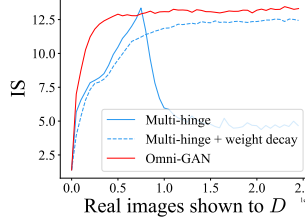


Figure 10: Weight decay can eliminate the early collapse problem of Multi-hinge GAN on CIFAR100.

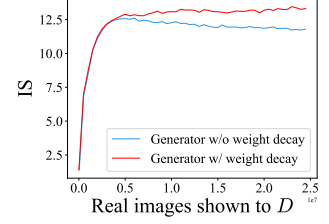


Figure 11: Applying weight decay to the generator. Experiments are conducted on CIFAR100.

Omni-GAN. We also did experiments on CIFAR10 (see Appendix D), and the results also showed the same trend. In addition, considering that Omni-GAN is more versatile than Multi-hinge GAN (e.g., Omni-GAN supports multiple positive labels, while Multi-hinge GAN only supports one positive label), we recommend considering Omni-GAN first when choosing cGANs.

5.4. How to Set the Weight Decay?

We did a grid search on the weight decay and found that its value is related to the size of the training dataset. For CIFAR100, there are only 500 images per class, and the weight decay is set to 0.0005. For CIFAR10, there are 5000 images per class, and the weight decay is set to 0.0001. For ImageNet, it is a large dataset with a considerable number of training data (approximate 1.2M). The weight decay is set to 0.00001. The conclusion is that the smaller the dataset, the higher the risk of over-fitting for the discriminator. Then weight decay should be larger.

5.5. Weight Decay for Generator

We found empirically that applying weight decay also to the generator can make training more stable. As shown in Fig. 11, although only applying weight decay to the discriminator can avoid the risk of collapse earlier, the IS has a trend of gradually decreasing as the training progresses. Fortunately, applying weight decay (set to be 0.001 in our experiments) to the generator can solve this problem. This phenomenon seems to indicate that the generator also has an over-fitting problem.

6. Conclusion

This paper presents an elegant and practical solution to training effective conditional GAN models. The key discovery is that strong supervision can largely improve the upper-bound of image generation quality, but it also makes the model prone to over-fitting. We design the **Omni-GAN** algorithm that equips the classification-based loss with regularization (in particular, weight decay) to alleviate over-fitting. Our algorithm achieves notable accuracy gains in a

few scenarios. Our research implies that there may be more ‘secrets’ in optimizing cGAN models. We look forward to applying the proposed algorithm to more scenarios and investigating further properties to improve cGAN.

References

- [1] Martin Arjovsky, Soumith Chintala, and Léon Bottou. Wasserstein Generative Adversarial Networks. In *ICML*, 2017. [1](#)
- [2] Andrew Brock, Jeff Donahue, and Karen Simonyan. Large scale gan training for high fidelity natural image synthesis. *arXiv:1809.11096*, 2018. [1](#), [4](#), [6](#), [7](#)
- [3] Minghao Chen, Shuai Zhao, Haifeng Liu, and Deng Cai. Adversarial-Learned Loss for Domain Adaptation. In *AAAI*, 2020. [1](#)
- [4] Qifeng Chen and Vladlen Koltun. Photographic Image Synthesis with Cascaded Refinement Networks. In *ICCV*, 2017. [6](#)
- [5] Marius Cordts, Mohamed Omran, Sebastian Ramos, Timo Rehfeld, Markus Enzweiler, Rodrigo Benenson, Uwe Franke, Stefan Roth, and Bernt Schiele. The Cityscapes Dataset for Semantic Urban Scene Understanding. In *CVPR*, 2016. [2](#), [8](#)
- [6] Harm de Vries, Florian Strub, Jérémie Mary, Hugo Larochelle, Olivier Pietquin, and Aaron Courville. Modulating early visual processing by language. In *NeurIPS*, 2017. [2](#)
- [7] Jia Deng, Wei Dong, Richard Socher, Li-Jia Li, Kai Li, and Li Fei-Fei. ImageNet: A large-scale hierarchical image database. In *CVPR*, Miami, FL, 2009. [2](#), [7](#)
- [8] Emily Denton, Soumith Chintala, Arthur Szlam, and Rob Fergus. Deep Generative Image Models using a Laplacian Pyramid of Adversarial Networks. *arXiv:1506.05751 [cs]*, 2015. [2](#)
- [9] Vincent Dumoulin, Jonathon Shlens, and Manjunath Kudlur. A Learned Representation For Artistic Style. In *ICLR*, 2017. [2](#)
- [10] Ian Goodfellow, Jean Pouget-Abadie, Mehdi Mirza, Bing Xu, David Warde-Farley, Sherjil Ozair, Aaron Courville, and Yoshua Bengio. Generative Adversarial Nets. In *NeurIPS*, 2014. [1](#)
- [11] Martin Heusel, Hubert Ramsauer, Thomas Unterthiner, Bernhard Nessler, and Sepp Hochreiter. GANs Trained by a Two Time-Scale Update Rule Converge to a Local Nash Equilibrium. In *NeurIPS*, 2017. [5](#)
- [12] Xun Huang and Serge Belongie. Arbitrary Style Transfer in Real-time with Adaptive Instance Normalization. In *ICCV*, 2017. [2](#)
- [13] Phillip Isola, Jun-Yan Zhu, Tinghui Zhou, and Alexei A. Efros. Image-to-Image Translation with Conditional Adversarial Networks. In *CVPR*, 2017. [5](#)
- [14] Xiang Jiang, Qicheng Lao, Stan Matwin, and Mohammad Havaei. Implicit Class-Conditioned Domain Alignment for Unsupervised Domain Adaptation. In *ICML*, 2020. [1](#)
- [15] Tero Karras, Timo Aila, Samuli Laine, and Jaakko Lehtinen. Progressive Growing of GANs for Improved Quality, Stability, and Variation. *arXiv:1710.10196 [cs, stat]*, 2017. [1](#), [6](#)
- [16] Tero Karras, Miika Aittala, Janne Hellsten, Samuli Laine, Jaakko Lehtinen, and Timo Aila. Training Generative Adversarial Networks with Limited Data. *arXiv:2006.06676 [cs, stat]*, 2020. [1](#), [4](#), [5](#), [6](#)
- [17] Tero Karras, Samuli Laine, and Timo Aila. A Style-Based Generator Architecture for Generative Adversarial Networks. In *CVPR*, 2019. [1](#)
- [18] Tero Karras, Samuli Laine, Miika Aittala, Janne Hellsten, Jaakko Lehtinen, and Timo Aila. Analyzing and Improving the Image Quality of StyleGAN. *arXiv:1912.04958 [cs, eess, stat]*, 2019. [1](#), [6](#)
- [19] Ilya Kavalero, Wojciech Czaja, and Rama Chellappa. cGANs with Multi-Hinge Loss. *arXiv:1912.04216 [cs, stat]*, 2019. [1](#), [3](#), [6](#)
- [20] Alex Krizhevsky, Geoffrey Hinton, et al. Learning multiple layers of features from tiny images. Technical report, Cite-seer, 2009. [2](#), [4](#)
- [21] Yann LeCun, Léon Bottou, Yoshua Bengio, Patrick Haffner, et al. Gradient-based learning applied to document recognition. *Proceedings of the IEEE*, 86(11), 1998. [2](#), [8](#)
- [22] Mingsheng Long, Zhangjie Cao, Jianmin Wang, and Michael I. Jordan. Conditional Adversarial Domain Adaptation. In *NeurIPS*, 2018. [1](#)
- [23] Mehdi Mirza and Simon Osindero. Conditional Generative Adversarial Nets. *arXiv:1411.1784 [cs, stat]*, 2014. [1](#), [2](#)
- [24] Takeru Miyato, Toshiki Kataoka, Masanori Koyama, and Yuichi Yoshida. Spectral Normalization for Generative Adversarial Networks. *arXiv:1802.05957 [cs, stat]*, 2018. [1](#), [6](#)
- [25] Takeru Miyato and Masanori Koyama. cGANs with Projection Discriminator. In *ICLR*, 2018. [1](#), [3](#), [4](#), [6](#)
- [26] Yuval Netzer, Tao Wang, Adam Coates, Alessandro Bis-sacco, Bo Wu, and Andrew Y Ng. Reading digits in natural images with unsupervised feature learning. 2011. [2](#), [8](#)
- [27] Augustus Odena, Christopher Olah, and Jonathon Shlens. Conditional Image Synthesis With Auxiliary Classifier GANs. *arXiv:1610.09585 [cs, stat]*, 2017. [1](#), [3](#), [6](#)
- [28] Taesung Park, Ming-Yu Liu, Ting-Chun Wang, and Jun-Yan Zhu. Semantic Image Synthesis with Spatially-Adaptive Normalization. In *CVPR*, 2019. [5](#), [6](#), [8](#)
- [29] Guim Perarnau, Joost van de Weijer, Bogdan Raducanu, and Jose M. Álvarez. Invertible Conditional GANs for image editing. *arXiv:1611.06355 [cs]*, 2016. [2](#)
- [30] Xiaojuan Qi, Qifeng Chen, Jiaya Jia, and Vladlen Koltun. Semi-parametric Image Synthesis. In *CVPR*, 2018. [5](#)
- [31] Scott Reed, Zeynep Akata, Xinchun Yan, Lajanugen Logeswaran, Bernt Schiele, and Honglak Lee. Generative Adversarial Text to Image Synthesis. In *ICML*, 2016. [2](#)
- [32] Masaki Saito, Eiichi Matsumoto, and Shunta Saito. Temporal Generative Adversarial Nets with Singular Value Clipping. In *ICCV*, 2017. [2](#)
- [33] Tim Salimans, Ian Goodfellow, Wojciech Zaremba, Vicki Cheung, Alec Radford, Xi Chen, and Xi Chen. Improved Techniques for Training GANs. In *NeurIPS*, 2016. [1](#), [5](#)
- [34] Florian Schroff, Dmitry Kalenichenko, and James Philbin. FaceNet: A Unified Embedding for Face Recognition and Clustering. In *CVPR*, 2015. [3](#)

- [35] Jianlin Su. Extending Cross-Entropy of Softmax to Multi-Label Classification. <https://kexue.fm/archives/7359>, 2020. 1, 8
- [36] Yifan Sun, Changmao Cheng, Yuhan Zhang, Chi Zhang, Liang Zheng, Zhongdao Wang, and Yichen Wei. Circle Loss: A Unified Perspective of Pair Similarity Optimization. In *CVPR*, 2020. 3, 8
- [37] Christian Szegedy, Vincent Vanhoucke, Sergey Ioffe, Jonathon Shlens, and Zbigniew Wojna. Rethinking the Inception Architecture for Computer Vision. *arXiv:1512.00567 [cs]*, 2015. 6
- [38] Eric Tzeng, Judy Hoffman, Kate Saenko, and Trevor Darrell. Adversarial Discriminative Domain Adaptation. *arXiv:1702.05464 [cs]*, 2017. 1
- [39] Ting-Chun Wang, Ming-Yu Liu, Jun-Yan Zhu, Guilin Liu, Andrew Tao, Jan Kautz, and Bryan Catanzaro. Video-to-Video Synthesis. In *NeurIPS*, 2018. 5
- [40] Ting-Chun Wang, Ming-Yu Liu, Jun-Yan Zhu, Andrew Tao, Jan Kautz, and Bryan Catanzaro. High-Resolution Image Synthesis and Semantic Manipulation with Conditional GANs. In *CVPR*, 2018. 5, 6
- [41] Fisher Yu, Vladlen Koltun, and Thomas Funkhouser. Dilated Residual Networks. In *CVPR*, Honolulu, HI, 2017. 8
- [42] Han Zhang, Tao Xu, Hongsheng Li, Shaoting Zhang, Xiaogang Wang, Xiao lei Huang, and Dimitris Metaxas. Stack-GAN: Text to Photo-realistic Image Synthesis with Stacked Generative Adversarial Networks. In *ICCV*, 2017. 2
- [43] Yang Zhao, Chunyuan Li, Ping Yu, Jianfeng Gao, and Changyou Chen. Feature Quantization Improves GAN Training. *arXiv:2004.02088 [cs, stat]*, 2020. 6
- [44] Peng Zhou, Lingxi Xie, Xiaopeng Zhang, Bingbing Ni, and Qi Tian. Searching towards Class-Aware Generators for Conditional Generative Adversarial Networks. *arXiv:2006.14208 [cs]*, 2020. 2

Omni-GAN: On the Secrets of cGANs and Beyond

Supplementary Material

A. FID Results of GANs and cGANs on CIFAR100

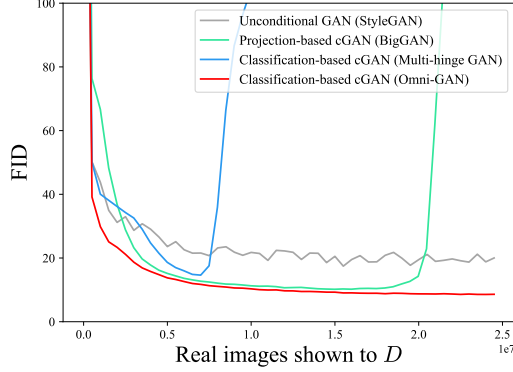


Figure 12: FID of unconditional GANs and conditional GANs (cGANs) on CIFAR100

We compared the IS of unconditional GANs and conditional GANs (cGANs) in Fig. 1 (in the paper). Their corresponding FID curves are shown in Fig. 12. As can be seen, the unconditional GAN, namely StyleGAN, is inferior to cGANs. Among the cGANs, both BigGAN and Multi-hinge GAN suffer from mode collapse. Omni-GAN not only achieves superior FID, but also enjoys a safe optimization process.

B. Multi-label Discriminator

We constructed a mixed cross-domain datasets by merging two datasets, MNIST and SVHN, which consist of images of digits from different domains. Some example images from the datasets are shown in Fig. 13. Let us take images of MNIST as an example, and show how to set the loss of the discriminator. As for SVHN, the case is analogous. Suppose \mathbf{x}_{real} is an image sampled from MNIST, we set the multi-label vector for \mathbf{x}_{real} as

$$\mathbf{y}_{\text{real}} = [\underbrace{0, \dots, 1_{\text{gt}}, \dots, 0}_{\text{class}}, \underbrace{1_{\text{mnist}}, 0}_{\text{domain}}, \underbrace{1_{\text{real}}, 0}_{\text{reality}}], \quad (16)$$

where 0 means the corresponding score belongs to the negative set, and 1 to the positive set. As can be seen, \mathbf{y}_{real} possesses three positive labels. The multi-label vector for \mathbf{x}_{fake} is then given by

$$\mathbf{y}_{\text{fake}} = [\underbrace{0, \dots, 0, \dots, 0}_{\text{class}}, \underbrace{0, 0}_{\text{domain}}, \underbrace{0, 1_{\text{fake}}}_{\text{reality}}], \quad (17)$$



(a) MNIST

(b) SVHN

Figure 13: Real images sampled from the dataset.



(a) MNIST

(b) SVHN

Figure 14: Images generated by a generator which is guided by a multi-label discriminator.

which is a one-hot vector with the last element being 1. The discriminator loss is the same as that defined in the paper (Eq. (10)).

For generator, its goal is to cheat the discriminator. We thus let the multi-label vector for \mathbf{x}_{fake} be

$$\mathbf{y}_{\text{fake}}^{(G)} = [\underbrace{0, \dots, 1_G, \dots, 0}_{\text{class}}, \underbrace{1_{\text{mnist}}, 0}_{\text{domain}}, \underbrace{1_{\text{real}}, 0}_{\text{reality}}], \quad (18)$$

where 1_G is 1 if its index in the vector is equal to the label adopted by the generator to generate \mathbf{x}_{fake} , otherwise 0. The generator loss is the same as that defined in the paper (Eq. (12)).

We experimentally found that this multi-label discriminator can indeed instruct the generator to generate images from different domains. Some generated images are shown in Fig. 14. We must emphasize that this is only a preliminary experiment to verify the function of the multi-label discriminator. We think that the multi-label discriminator have a potential to be employed in other tasks in the future, such

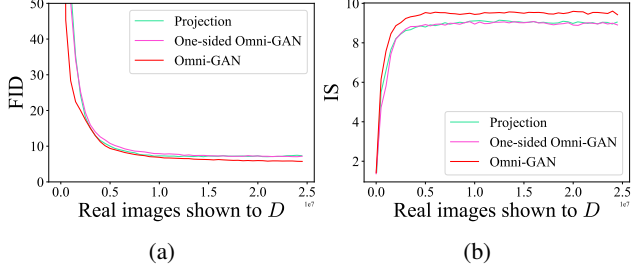


Figure 15: The performance of one-sided Omni-GAN is on par with that of projection-based GAN on CIFAR10.

as translation between images in different domains, domain adaptation, *etc.*

C. Comparison of One-sided Omni-GAN and Projection-based GAN on CIFAR10

We provide the results of one-sided Omni-GAN and projection-based GAN (in particular, BigGAN) on CIFAR10. As shown in Fig. 15, one-sided Omni-GAN is comparable to the projection-based GAN in terms of both FID and IS. The reason is that one-sided Omni-GAN utilizes class supervision in the same way as projection-based GAN. However, both one-sided Omni-GAN and projection-based GAN are inferior to Omni-GAN. Because the only difference between one-sided Omni-GAN and Omni-GAN is whether the supervision is fully utilized, we can easily conclude that the superiority of Omni-GAN lies in the full use of supervision.

D. Combining Multi-hinge GAN with Weight Decay

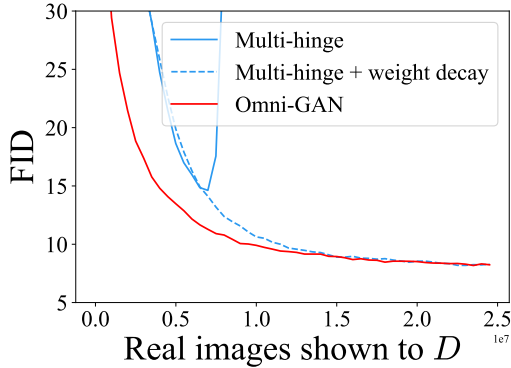


Figure 16: FID on CIFAR100. Combining Multi-hinge GAN with weight decay can avoid collapsing earlier.

We found that weight decay is still effective for Multi-hinge GAN. Fig. 16 shows the FID curves on CIFAR100. Original Multi-hinge GAN suffers a severe early collapse

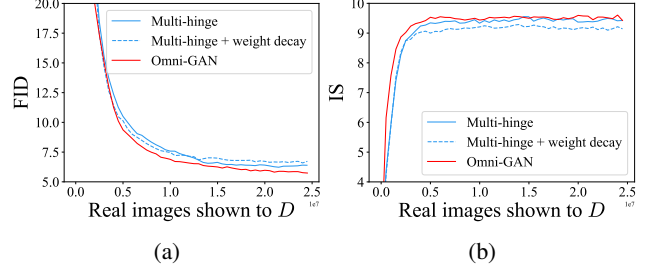


Figure 17: Combine Multi-hinge GAN with weight decay on CIFAR10. Weight decay deteriorates Multi-hinge GAN.

issue because it employs strong class supervision. After equipped with weight decay, Multi-hinge GAN enjoys a safe optimization and its FID is even comparable to that of Omni-GAN.

Multi-hinge GAN combined with weight decay does not always perform well. The results on CIFAR10 are shown in Fig. 17. To our surprise, weight decay deteriorates Multi-hinge GAN in terms of both FID and IS. The reason for this is unknown. On the other hand, Omni-GAN, employing weight decay by default, achieves superior performance. In addition, Omni-loss is more flexible than multi-hinge loss. For example, it can be easily degraded to a projection-based cGAN, and supports multi-label classification. As a result, we suggest first considering using Omni-GAN when choosing cGAN models.

E. Applying Weight Decay to the Generator

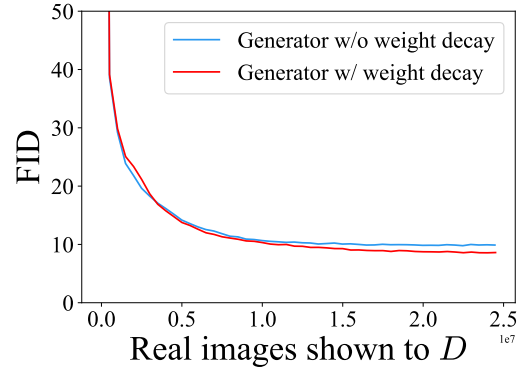


Figure 18: FID curves with or without weight decay for the generator. Experiments are conducted on CIFAR100.

In the paper, we showed that applying weight decay to the generator can make the training process more stable. We provide the FID curves in Fig. 18. It can be seen that applying weight decay to the generator can slightly improve performance in terms of FID. To sum up, applying weight decay to the discriminator can avoid collapse during training. Applying weight decay to the generator at the same

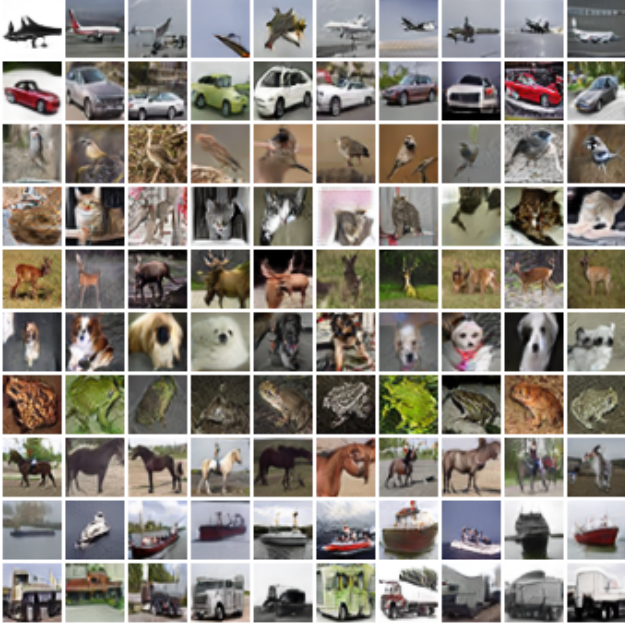


Figure 19: Randomly generated image by Omni-GAN for CIFAR10

time can improve the performance of the generation.

F. Additional Results

F.1. Generated Images on CIFAR and ImageNet

In Fig. 19, 20 and 21, we show generated images from Omni-GAN on CIFAR10, CIFAR100, and ImageNet datasets respectively. Due to limited space, we only show images of some categories on CIFAR100 and ImageNet.

F.2. Results of Semantic Image Synthesis

In Fig. 22, we show several results of Omni-GAN as well as those of SPADE for semantic image synthesis. The label maps and the ground truth images are from the first ten items in the test set of Cityscapes dataset, without cherry-picking.

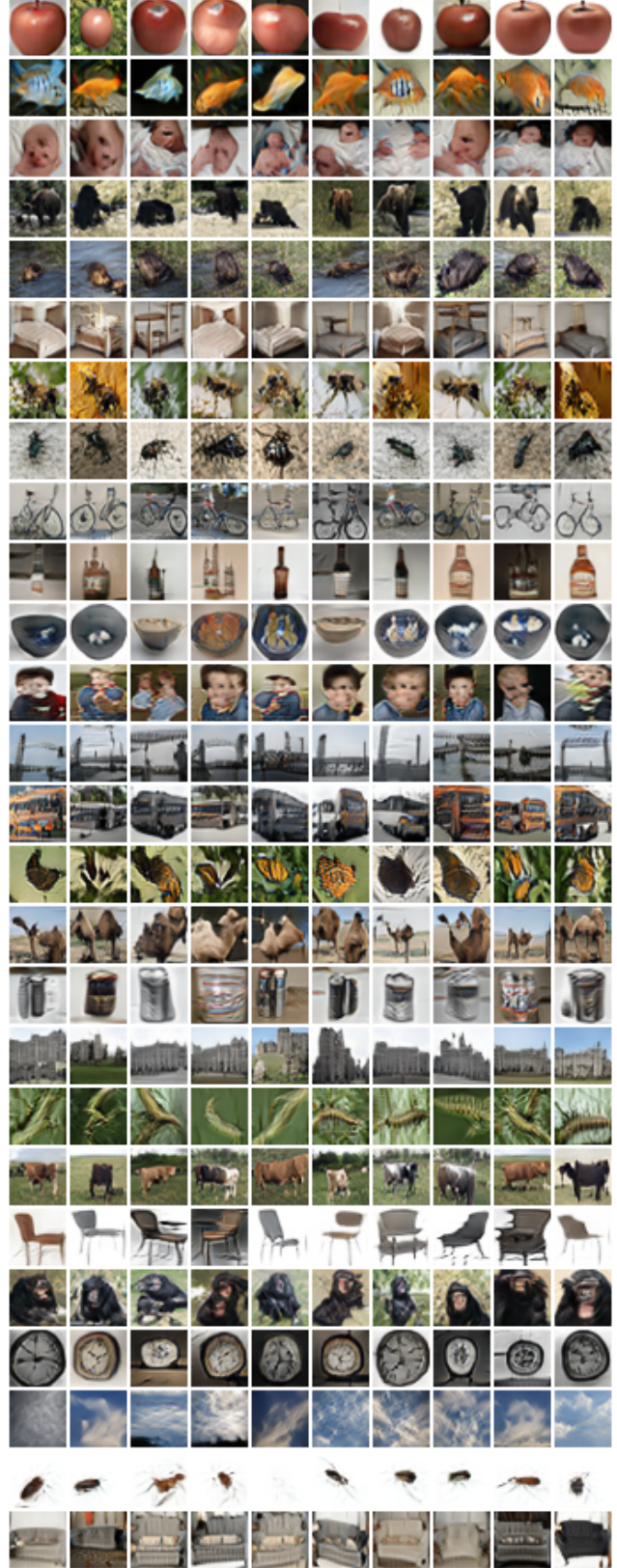


Figure 20: Randomly generated image by Omni-GAN for CIFAR100

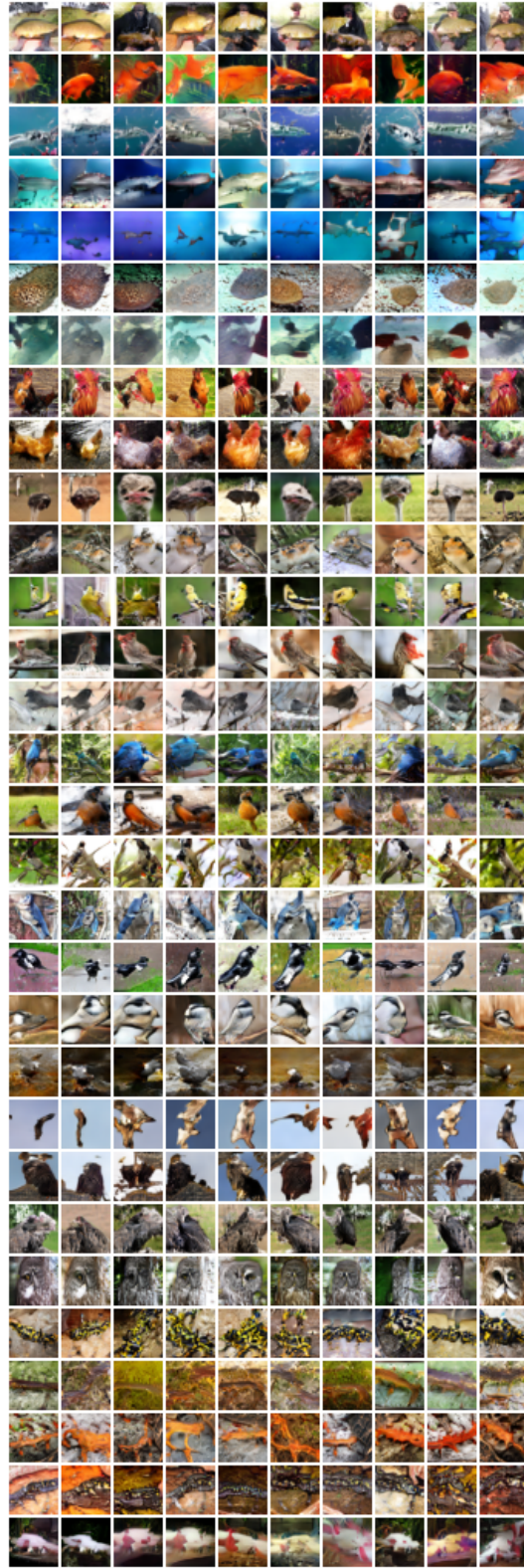


Figure 21: Randomly generated image by Omni-GAN for ImageNet 32×32 .

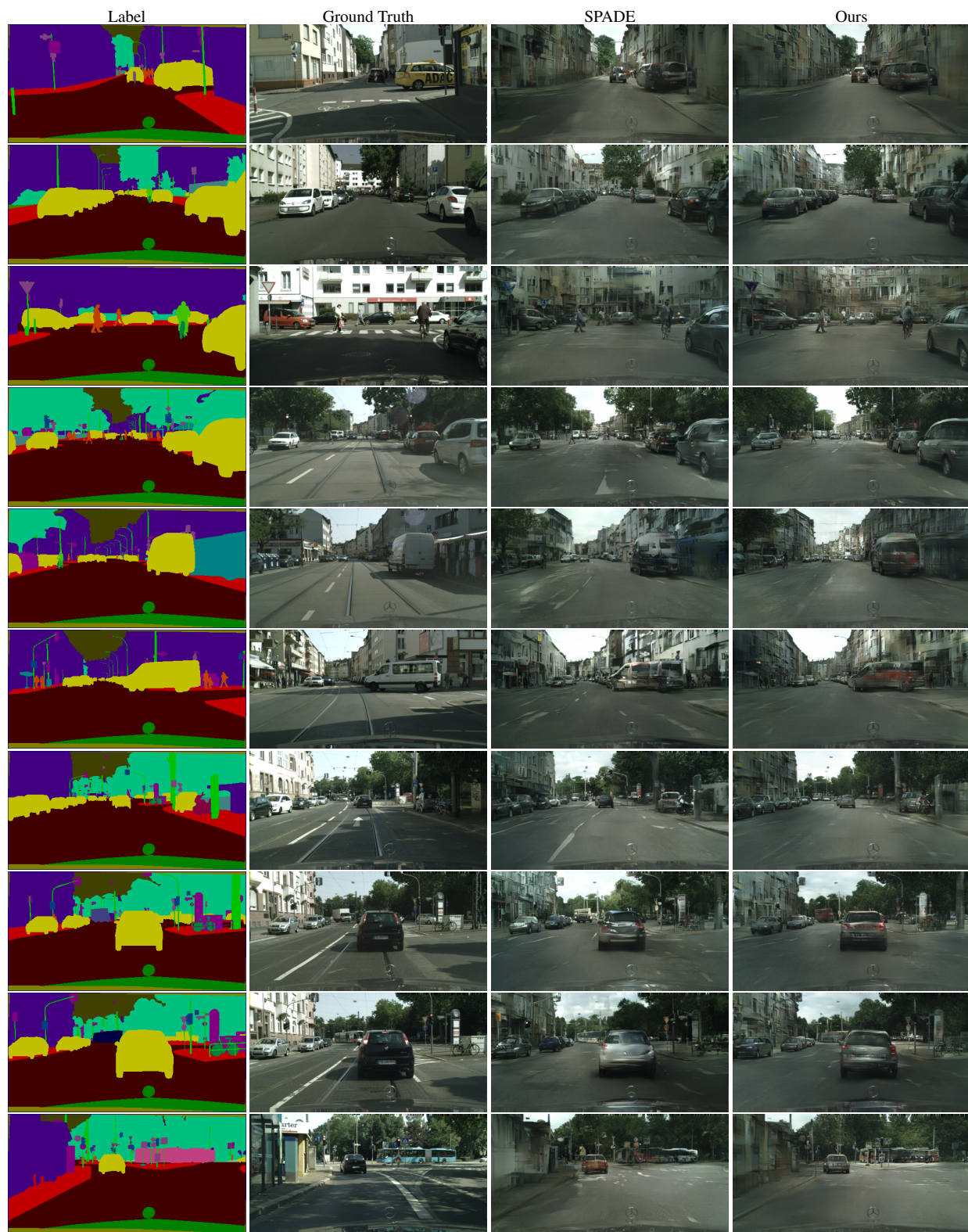


Figure 22: Results of semantic image synthesis on Cityscapes.